Supporting Information For

Activating discharge and inhibiting self-corrosion by adding indium to the anode of Mg-air battery

Donghu Li[a], Lifeng Hou[a,b*], Huayun Du[a,b], Huan Wei[b], Xiaoda Liu[b], Qian Wang[a,b*], Chengkai Yang[c*] and Yinghui Wei[a,b*]

[a] *College of Materials Science and Engineering, Taiyuan University of Technology, Taiyuan, 030024, Shanxi, China*

[b] *Corrosion and Protection Engineering Technology Research Center of Shanxi Province, Taiyuan, 030024, Shanxi, China*

[c] *Key Laboratory of Advanced Materials Technology, College of Materials Science and Engineering, Fuzhou University, Fuzhou 350108, Fujian, China*

*Corresponding authors.

Email address: houlifeng78@126.com (L. Hou); qianwang0825@pku.edu.cn (Q. Wang); chengkai_yang@fzu.edu.cn (C. Yang); yhwei_tyut@126.com (Y. Wei).

Experimental procedure

Materials and microstructural characterization

A variety of Mg-xIn (x=0.5, 1, 2 and 4 wt.%) binary alloys were melted using high-purity Mg (99.99 wt.%) and In (99.99 wt.%). Subsequently, the alloys were subjected to solid solution treatment, which consisted of quenching in water after holding at 450 °C for 12 h. The samples used for microstructure observation were carefully ground and polished. After that, samples were cleaned with anhydrous ethanol and etched with nitric acid solution (4 vol.% nitric acid in ethanol). The grain sizes of the samples were observed using an optical microscope (OM, Zeiss), and the phase composition of the samples was determined using X-ray diffraction (XRD, TD-3500). The actual compositions of pure Mg and Mg-In alloys were analyzed by Inductively Coupled Plasma-Optical Emission Spectroscopy (ICP-OES, Agilent 5110) and were listed in **Table S1**.

Electrochemical test

The potentiodynamic polarization curves and electrochemical impedance spectra (EIS) of the studied alloys were tested after the open circuit potential (OCP) had stabilized (30 min). The electrolyte was 3.5 wt.% NaCl solution. The EIS tests were performed with frequency range of 100 kHz to 0.05 Hz and a perturbation amplitude of ±5 mV. The results of EIS were fitted by Zview software. The potentiodynamic polarization curves were recorded at a scan rate of 1 mV s^{-1} with a scan range of -0.2 V/OCP to +0.5 V/OCP.

Mg-air battery discharge test

The discharge of Mg-air battery was evaluated using the Neware Battery Test System, and the special electrolytic cells for Mg-air batteries were purchased from Changsha Spring New Energy Technology co. ltd, with a fixed cathode area of 2×2 cm^2. The anodes tested were small 1×1×1 cm^3 blocks encapsulated in epoxy, and the cathodes were commercial air cathodes. The discharge voltage curves of all alloys were recorded and compared with the commercial AZ31 alloy (same heat treatment state as Mg-In alloys). Subsequently, the discharged samples were weighed after placing them in heated 200 g L^{-1} chromic acid solution to remove the discharge products, and then the anode efficiency, specific energy and discharge capacity of the alloys were calculated by the following equations (S1-S3):

$$\textit{Discharge efficiency (\%)} = \frac{3.6 \times i_d \times t \times A \times M}{2F \times \Delta W} \times 100\% \quad \text{(S1)}$$

$$\textit{Discharge capacity (mA h g - 1)} = \frac{i_d \times t \times A}{\Delta W} \quad \text{(S2)}$$

$$\textit{Specific energy (mW h g - 1)} = \frac{U \times i_d \times t \times A}{\Delta W} \quad \text{(S3)}$$

where i_d is the discharge current density (mA cm^{-2}), t is the discharge time (h), A is the surface area (1 cm^2), M is the molar mass (g mol^{-1}), F is the Faraday constant (26800 mAh mol^{-1}), ΔW is the mass loss after discharge (g) and U is the average discharge voltage (V). In addition, the surface morphologies and the cross-section morphologies of the alloys after discharge were observed by scanning electron microscopy (SEM, TESCAN VEGA3). And the discharge products were analyzed by XRD and XPS. Furthermore, long-time discharge, intermittent discharge and constant power discharge of Mg-1In and pure Mg are also tested to evaluate the performance of the battery during real life use.

Table S1. ICP results for the chemical composition of the Mg-In binary alloys (wt.%).

Materials	In	Fe	Cu	Si	Ni	Mg
Pure Mg	-	0.0018	0.0003	0.0016	<0.0003	Bal.
Mg-0.5In	0.50	0.0016	0.0003	0.0011	<0.0003	Bal.
Mg-1In	1.16	0.0010	0.0003	0.0014	<0.0003	Bal.
Mg-2In	2.24	0.0011	0.0005	0.0012	<0.0003	Bal.
Mg-4In	4.11	0.0008	0.0004	0.0009	<0.0003	Bal.

Table S2. The results of fitting EIS based on the equivalent circuit of **Fig. 1c**.

Alloys	R_s	CPE_1	n_1	R_{ct}	CPE_2	n_2	R_f	L	Chi-squared
	Ω cm^2	Ω cm^2 s^n		Ω cm^2	Ω cm^2 s^n		Ω cm^2	H cm^{-2}	
Pure Mg	9.24	5.82×10^{-5}	0.85	103.2	-	-	271.9	11.59	0.00686
Mg-0.5In	8.99	6.21×10^{-5}	0.86	252.3	-	-	37.9	1467	0.00212
Mg-1In	9.67	1.69×10^{-3}	0.73	632.8	1.12×10^{-5}	0.94	783.0	-	0.00187
Mg-2In	9.07	1.76×10^{-3}	0.71	505.8	1.46×10^{-5}	0.94	690.9	-	0.00096
Mg-4In	8.67	2.63×10^{-3}	0.71	404.2	1.21×10^{-5}	0.94	489.6	-	0.00217

Table S3. Fitting results of polarization curves.

Alloys	E_{corr}	I_{corr}
	V vs. SCE	μA cm^{-2}
Pure Mg	-1.564	169.82
Mg-0.5In	-1.591	36.69
Mg-1In	-1.741	5.86
Mg-2In	-1.715	13.16
Mg-4In	-1.714	26.99

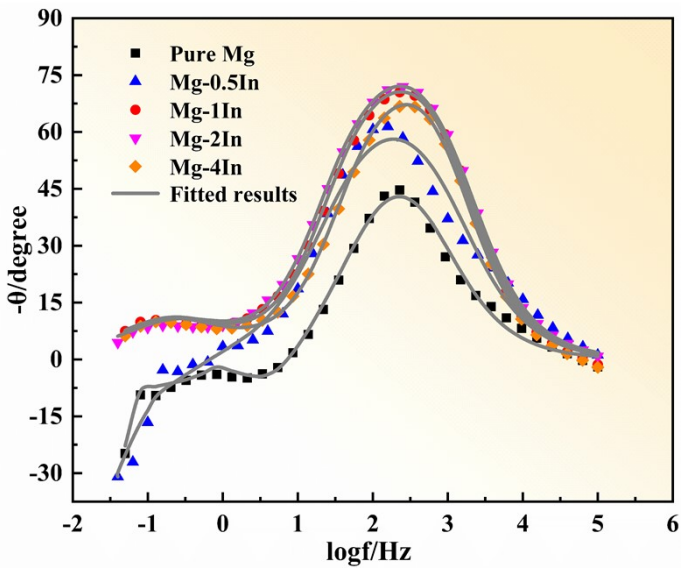

Fig. S1. The results of electrochemical impedance spectra: Bode plots of phase angle vs. frequency.

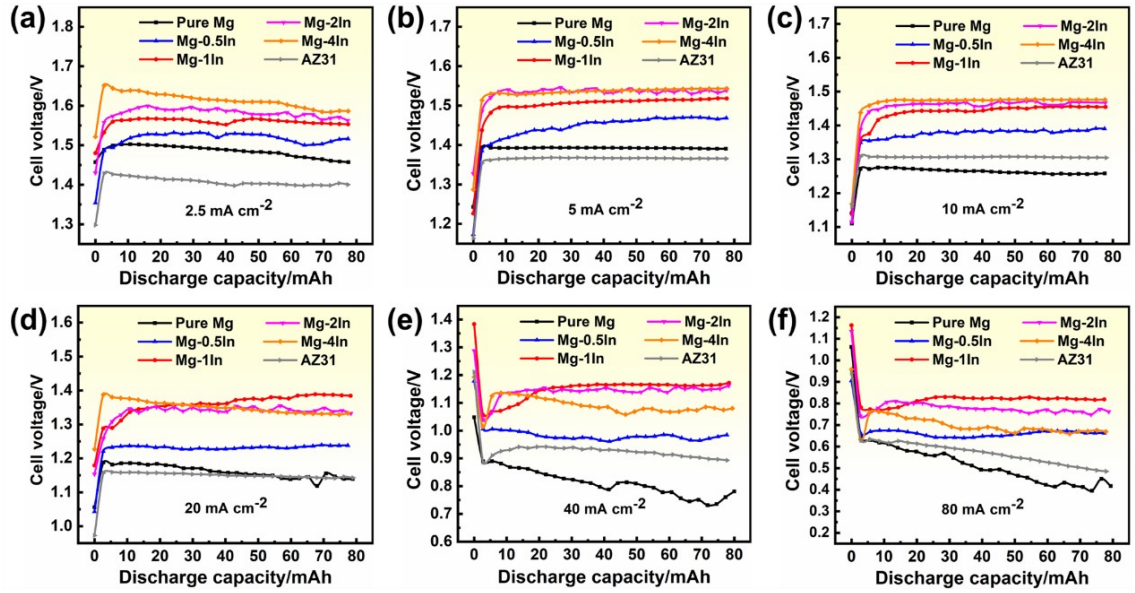

Fig. S2. Galvanostatic discharge curves (cell voltage vs. discharge capacity) of the studied anodes and commercial AZ31 alloy for Mg-air batteries in 3.5 wt.% NaCl solution: (a) 2.5 mA cm^{-2}; (b) 5 mA cm^{-2}; (c) 10 mA cm^{-2}; (d) 20 mA cm^{-2}; (e) 40 mA cm^{-2}; (f) 80 mA cm^{-2}.

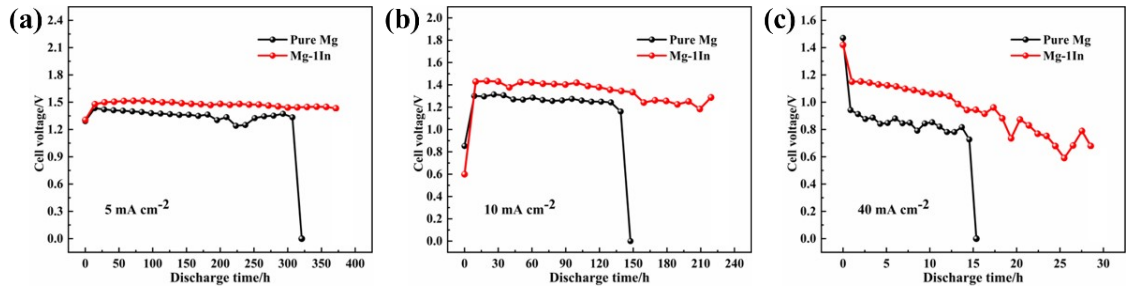

Fig. S3. Long-time discharge curves of pure Mg and Mg-1In alloys at different current densities in 3.5 wt.% NaCl solution: (a) 5 mA cm^{-2}, (b) 10 mA cm^{-2}, (c) 40 mA cm^{-2}.

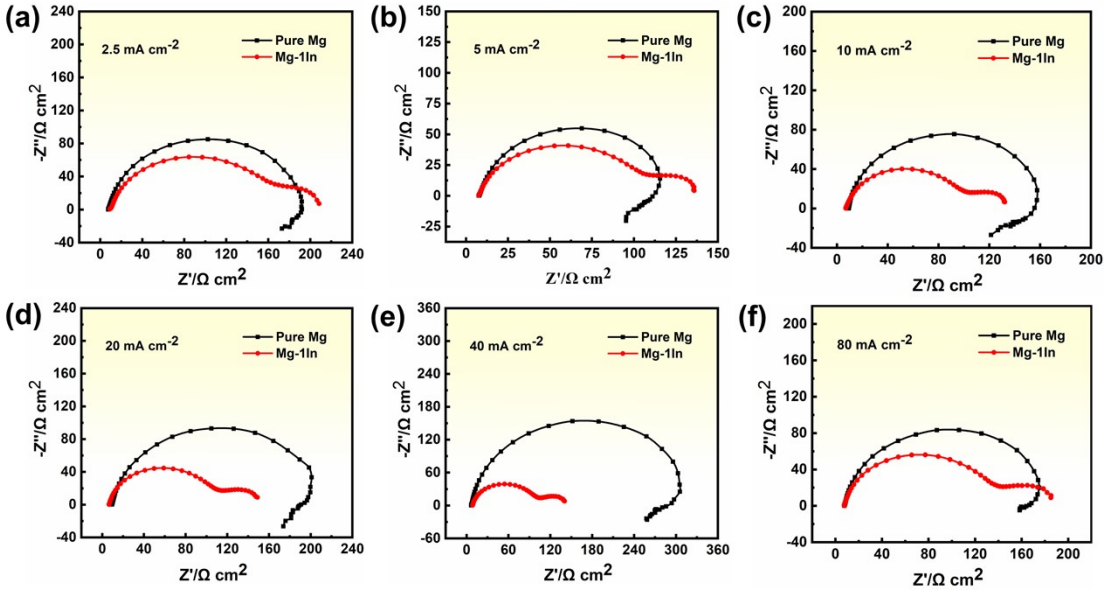

Fig. S4. The EIS tests of pure Mg and Mg-1In alloys after discharge of 80 mAh at different current densities: (a) 2.5 mA cm^{-2}, (b) 5 mA cm^{-2}, (c) 10 mA cm^{-2}, (d) 20 mA cm^{-2}, (e) 40 mA cm^{-2}, (f) 80 mA cm^{-2}.

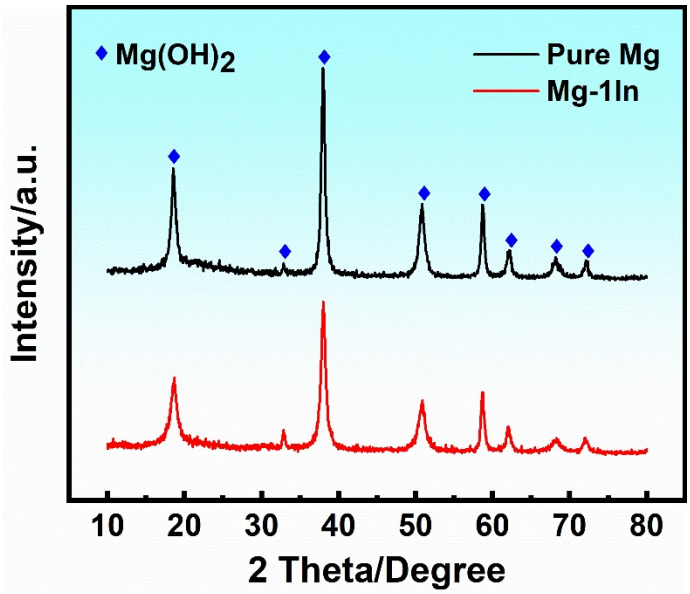

Fig. S5. XRD patterns for discharge products of pure Mg and Mg-1In alloy following discharge at 2.5 mA cm^{-2}.

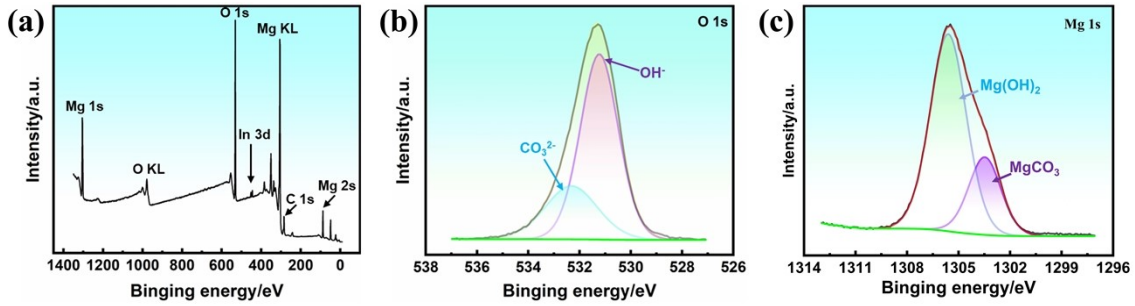

Fig. S6. XPS analysis for discharge products of Mg-1In alloy after discharging at 2.5 mA cm^{-2}.

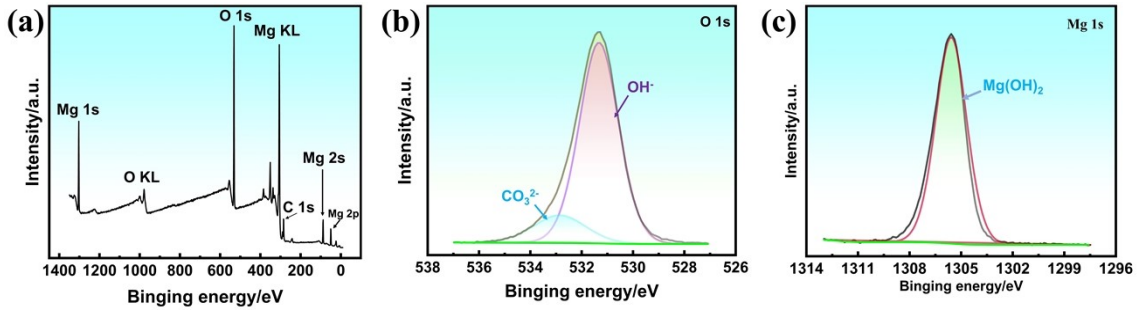

Fig. S7. XPS analysis for discharge products of pure Mg alloy after discharging at 2.5 mA cm^{-2}.

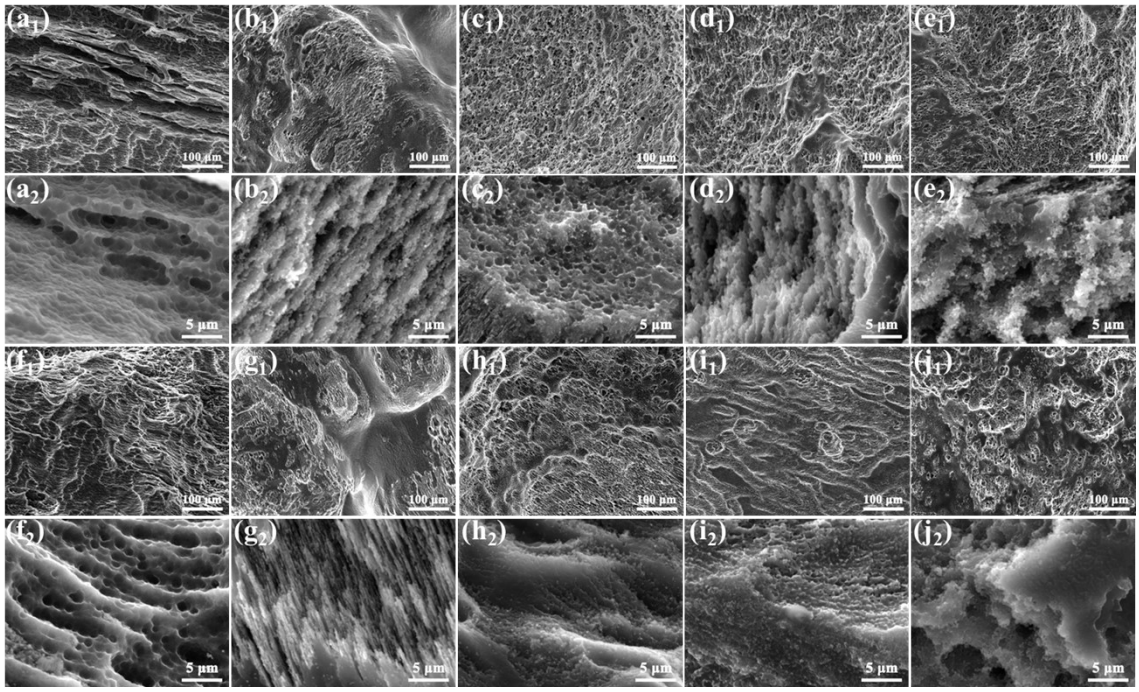

Fig. S8. Surface morphologies of pure Mg and Mg-In alloys without discharge products after discharge 80 mAh at 5 mA cm^{-2} (a-e) and 10 mA cm^{-2} (f-j) in 3.5 wt.% NaCl solution: (a, f) Pure Mg; (b, g) Mg-0.5In; (c, h) Mg-1In; (d, i) Mg-2In; (e, j) Mg-4In.

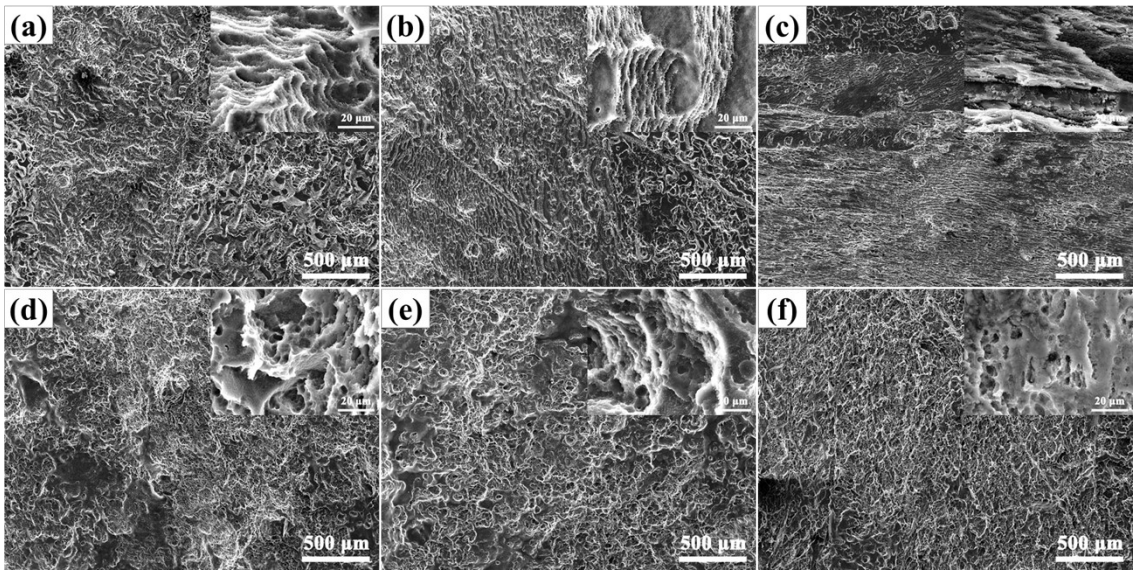

Fig. S9. Surface morphologies of pure Mg and Mg-In alloys without discharge products after discharge 80 mAh at 20 mA cm^{-2} (a, d), 40 mA cm^{-2} (b, e) and 80 mA cm^{-2} (c, f) in 3.5 wt.% NaCl solution: (a-c) Pure Mg; (d-f) Mg-1In.

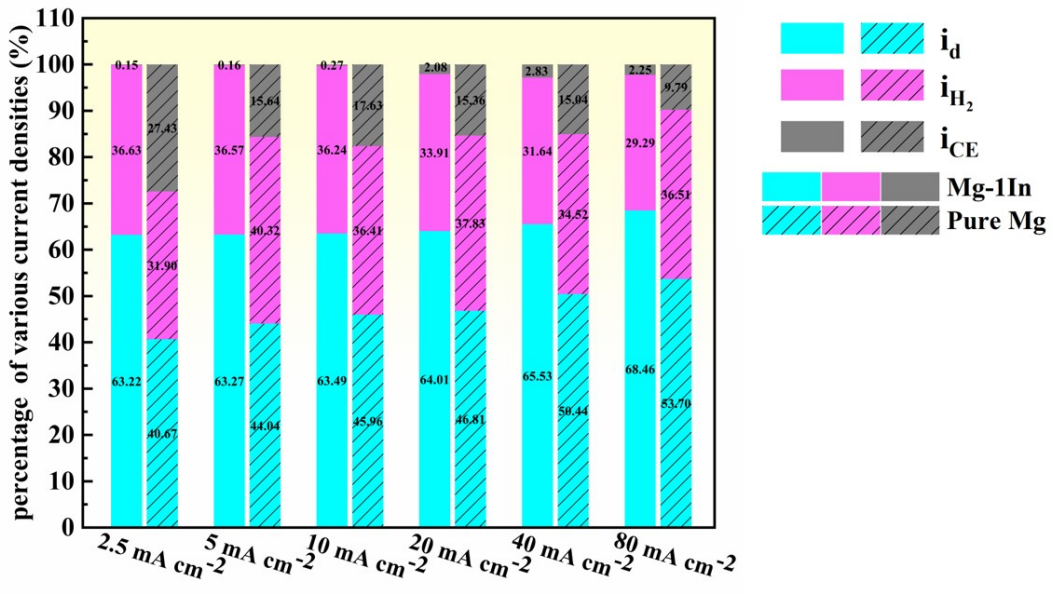

Fig. S10. Discharge current densities (i_d), hydrogen precipitation current densities (i_{H_2}), and weight loss current density caused by the chunk effect (i_{CE}) as a percentage of total current density (i_M) for pure Mg and Mg-1In alloys.

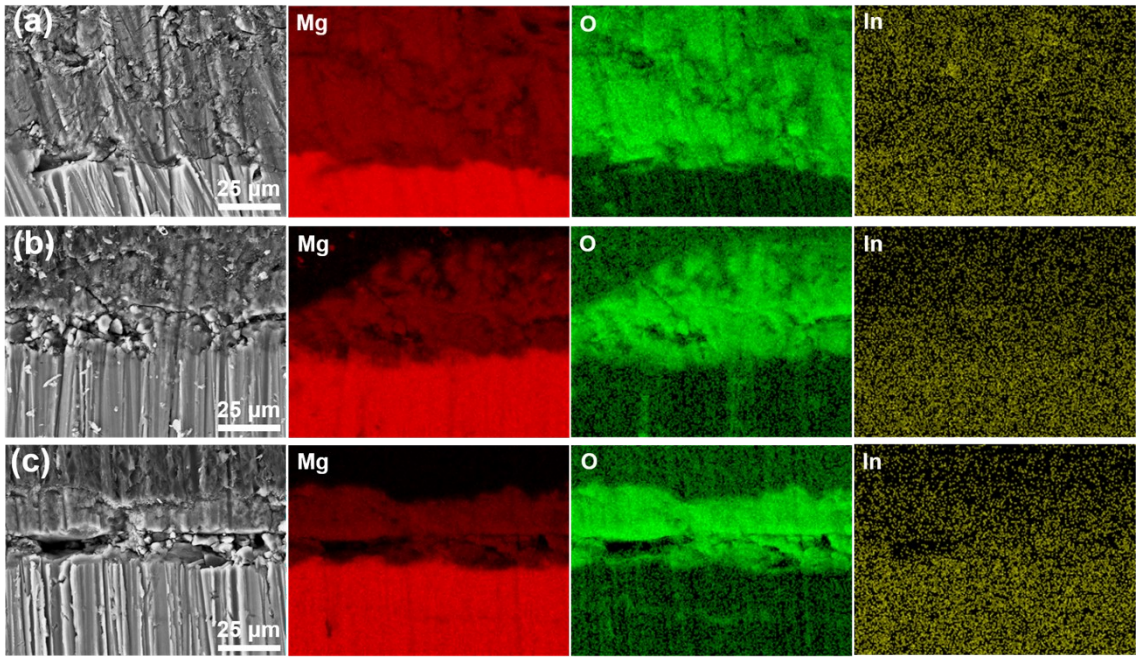

Fig. S11. The SEM morphologies of cross section and EDS surface scanning of Mg, O and In elements after discharge at different current densities of Mg-1In anodes: (a) 10 mA cm^{-2}; (b) 40 mA cm^{-2}; (c) 80 mA cm^{-2}.